DOI https://doi.org/10.30525/978-9934-26-254-8-10

ENERGY-EFFICIENT SERIES-RESONANT DC/DC CONVERTER

Pavlov H. V., Vinnychenko I. L., Pokrovskii M. V.

INTRODUCTION

A significant part of production equipment and high-tech systems of various purposes consume electricity in the converted form. The share of electric energy transmitted to electricity consumers through high-frequency pulse converters is constantly increasing. In this regard, the development and improvement of semiconductor converters (SC) of electricity, which provide a solution to energy saving tasks, becomes important. The development of SC occurs with ever-increasing requirements for the quality of the initial parameters, the level of energy losses and generated interference, as well as the specific mass and size indicators of the converters[1].

The use of resonant inverters in the NP allows providing such advantages as: improving the trajectories of turning on and off the power switches of the converter[2];

improvement of EMC by forming a partial sinusoidal current in the power section of the converter[3]; provision of various external characteristics specified by circuit solutions[4] or switching algorithms of power switches without changing the power section of the converter[5,6].

---

[1] Браун М. *Источники питания. Расчет и конструирование*. Киев: «МК-Пресс». 2007. С. 97.

[2] Bose B.K. *Modern Power Electronics and AC Drives*. PHI Learning Pvt Lt. 2013. P. 546.

[3] Dianbo Fu, Kong P., Wang S., Lee F. C., Ming Xu. Analysis and suppression of conducted EMI emissions for front-end LLC resonant DC/DC converters. *IEEE Power Electronics Specialists Conference.* 2008. P.1145.

[4] Pavlov, G., Obrubov, A., Vinnychenko, I. Design procedure of static characteristics of the resonant convertere. *Proc. of IEEE 3rd Ukraine Conference on Electrical and Computer Engineering (UKRCON).* 2021. P. 401.

[5] Zheng K., Zhang G., Zhou D., Li J., Yin S. Modeling, dynamic analysis and control design of full-bridge LLC resonant converters with sliding-mode and PI control scheme. *Journal of Power Electronics*. 2018. Vol. 18, no. 3. P. 766

[6] Rubavathy J., Murugesan P. Class D series resonant inverter with PDM scheme for induction heating application. *International Journal of Applied Engineering Research*. 2016. Vol. 11, no. 6. P. 3819

Thus, resonant switching principles provide a significant increase in the operating frequency of converters while maintaining or reducing the level of switching losses. Resonant converters generate a limited spectrum of electromagnetic interference, which favorably affects the EMC of converters with a power supply network and contributes to the wide application of this type of converters in autonomous conditions.

1. Research of energy exchange processes in the power circuit of a series-resonant direct current converter and its mathematical model

The power part of the series-resonant converter (SRC), which converts direct current into direct current, is a two-bridge converter, in which the M1 bridge and the series-resonant circuit perform the role of the resonant inverter, and the role of a rectifier is played by the M2 bridge (fig. 1).[7]*. The series-resonant circuit consists of* L_r, C_r, R_r, *where the resistance* R_r *represents the active losses of the resonant circuit and switches of switching bridges* M_1 *and* M_2*. The output filter of the converter is represented by the capacitor* C_f*. As a rule, the time constant of the SRC filter is much larger than the time constant of the resonant circuit. According to the compensation theorem, the load circuit can be replaced by an equivalent voltage source* U_{out}*. This makes it possible to study the dependence of the processes in the SRC on the values of the input* U_s *and output* U_{out} *voltages.*

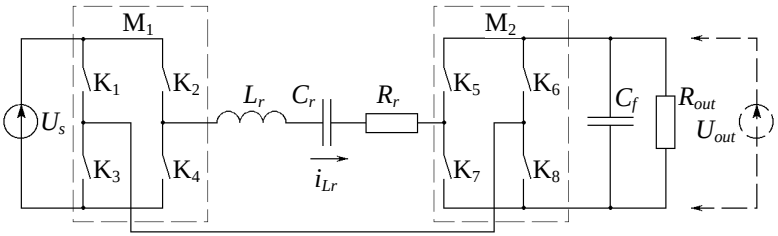

Fig. 1. The power section of series-resonant DC converter

The method of pulse-number control of the output parameters of the SRC ensures switching of the switches only at zero values of the resonant

[7] Павлов Г. В., Обрубов А. В., Нікітіна О. В., Покровський М. В. *Перетворювачі постійної напруги на основі резонансних інверторів: монографія*. Миколаїв: НУК. 2013. С. 98

current, which causes minimal switching losses[8]. To ensure this, the power switches of the resonant converter must conduct current during the whole number of half-periods of resonant oscillations. Then, during regulation, it is possible to control the energy exchange between the power source, the resonant circuit and the load by alternating three elementary algorithms for switching transistors or so called conversion phases. In the first switching algorithm, energy is transferred from the power source through the inverter (phase of direct energy transfer *Fr*), in the second – the power source does not participate in the energy exchange (energy dissipation phase *Ds*), in the third – energy enters the power source (phase of reverse energy transfer *Rv*). The change of phases must occur synchronously with the transitions of the resonant current through zero values.

During the half-period of oscillations, the voltage which is applied to the resonant circuit, is one of the combinations of input and output voltages, which depends on the phase of the conversion. Therefore, the resonant current curve has a shape close to sinusoidal. During the next half-period of oscillations, the voltage of the same magnitude, but with the opposite sign, is applied to the resonant circuit. If the directions of the resonant current and the voltage applied to the circuit coincide, the amplitude of the resonant current will increase, and if there is a discrepancy, it will decrease. In fig. 2. time diagrams of current i_{Lr} and voltage u_{Cr} in the circuit during the conversion phases mentioned above are given.

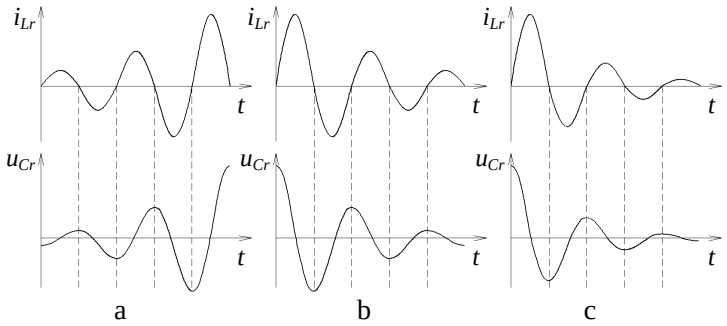

Fig. 2. Time diagrams of current and voltage in the circuit during the conversion phases: a – *Fr*; b – *Ds*; c – *Rv*

[8] Pavlov G., Pokrovskiy M., Vinnichenko I. Load characteristics of the serial-to-serial resonant converter with pulse-number regulation for contactless inductive energy transfer. *IEEE 3rd International Conference on Intelligent Energy and Power Systems (IEPS)*. 2018. P. 133.

During the *Fr* and *Rv* transformation phases a voltage is applied to the resonant circuit, which is a combination of U_s and U_{out}, the directions of which are the same or opposite to the direction of the resonant current, respectively. During the *Fr* phase *the switches are open.*

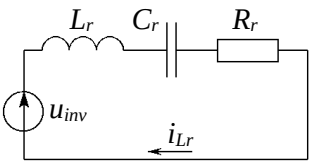

Fig. 3. Connecting the inverter to the resonant circuit

During the *Ds* transformation phase the voltage U_{out} is applied to the resonant circuit the direction of which is opposite to the direction of the resonant current. During the *Fr* phase, energy is transferred from the source to the load and the resonant circuit (fig. 2, a). During the *Ds* transformation phase energy is transferred from the circuit to the load (fig. 2, b), and in the *Rv* phase – from the circuit to the source and load (fig. 2, c). The operation of the SRC is possible with certain sequences of phase connections (PhC). Each PhC consists of several transformation phases. In the future, the combination of the transformation phases *Fr* and *Ds* (which will be called PhC I in the future) is considered.

Let's consider the processes that occur in the resonant circuit during thr pulse-number control. For this purpose, we will highlight the resonant circuit to which the inverter voltage is applied u_{inv} (fig. 3).

The voltage u_{inv} represents rectangular pulses (fig. 4) with amplitude U_{inv}, the polarity of which changes when the resonance current i_{Lr} polarity changes.

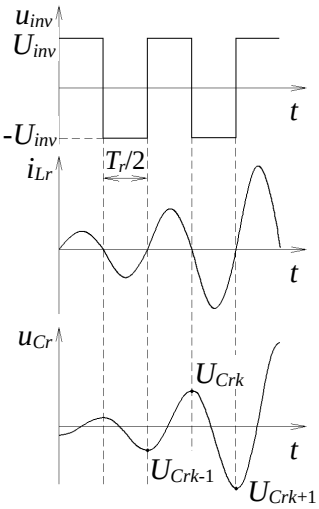

Fig. 4. Time diagrams of processes in a resonant circuit

The value U_{inv} depends on the conversional phase:

– in the phase *Fr*: $U_{inv} = U_{Fr} = U_s - U_{out}$;

– in the phase *Ds*: $U_{inv} = U_{Ds} = -U_{out}$;

– in the phase *Rv*: $U_{inv} = U_{Rv} = -U_s - U_{out}$.

The voltage on the resonant capacitor and the resonant current during the first half-period of the resonant oscillations are determined by the dependences:

$$u_{Cr}(t) = U_{inv} - (U_{inv} - U_{Cr0}) \cdot e^{-\delta t} \cdot \cos \omega t ,$$

$$i_{Lr}(t) = \frac{U_{inv} - U_{Cr0}}{\rho} \cdot e^{-\delta t} \cdot \sin \omega t ,$$

where U_{Cr0} – the voltage on the resonant capacitor at the beginning of the conversion cycle, which consists of a certain number of half-periods of resonant oscillations; $\rho = \sqrt{L_r / C_r}$ – wave resistance of the circuit; δ – damping factor.

During the second half-period of resonant oscillations, voltage and current are determined by dependencies:

$$u_{Cr}(t) = -U_{inv} + (U_{inv} + U_{Cr1}) \cdot e^{-\delta t} \cdot \cos \omega t ,$$

$$i_{Lr}(t) = \frac{-U_{inv} - U_{Cr1}}{\rho} \cdot e^{-\delta t} \cdot \sin \omega t ,$$

where U_{Cr1} – voltage of the capacitor after the first half-period.

Expression for the capacitor voltage U_{Cr} in the end of *k*-th half-period:

$$U_{Crk} = \left[\Theta^k U_{Cr0} - U_{inv} \left(1 - \Theta^k + 2 \sum_{i=1}^{k} \Theta^i \right) \right] \cdot (-1)^k ,$$

where $\Theta = e^{-\delta \frac{T_r}{2}}$ – attenuation per half-period; T_r – period of resonant oscillations.

Consider the process consisting of the transformation phases *Fr* and *Ds*. Each phase of the transformation contains a certain number of half-

periods of resonant oscillations, respectively n_{Fr} and n_{Ds}. The total number of half-periods of resonant oscillations per conversion cycle $n = n_{Fr} + n_{Ds}$ must be even so that the resonant capacitor voltage at the beginning and at the end of the conversion period has the same polarity. To ensure the energy balance, it is necessary to fulfill the condition $U_{Cr\text{n}} = U_{Cr0}$:

$$U_{Crn} = \left\{ \left[\Theta^{n_{Fr}} U_{Ct0} - U_{Fr} \left(1 - \Theta^{n_{Fr}} + 2 \sum_{i=1}^{n_{Fr}} \Theta^i \right) \right] (-1)^{n_{Fr}} \Theta^{n_{Ds}} - \right.$$
$$\left. - U_{Ds} (-1)^{n_{Fr}} \left(1 - \Theta^{n_{Ds}} + 2 \sum_{i=1}^{n_{Ds}} \Theta^i \right) \right\} (-1)^{n_{Ds}}, \quad (1)$$

where $U_{Cr\text{n}}$ –the resonant capacitor voltage at the end of the conversion cycle: U_{Fr} and U_{Ds} – he voltage on the resonant capacitor at the end of the conversion cycle of the voltages applied to the circuit during the *Fr* and *Ds* phases, respectively.

After transformation (1), we get:

$$U_{Cr0} \left(1 - \Theta^n \right) = -U_{Fr} \left(1 - \Theta^{n_{Fr}} + 2 \sum_{i=1}^{n_{Fr}} \Theta^i \right) \Theta^{n_{Ds}} - U_{Ds} \left(1 - \Theta^{n_{Ds}} + 2 \sum_{i=1}^{n_{Ds}} \Theta^i \right) =$$
$$= \left(U_{out} - U_s \right) \left(1 - \Theta^{n_{Fr}} + 2 \sum_{i=1}^{n_{Fr}} \Theta^i \right) \Theta^{n_{Ds}} + U_{out} \left(1 - \Theta^{n_{Ds}} + 2 \sum_{i=1}^{n_{Ds}} \Theta^i \right).$$

After entering the designation $q = U_{out} / U_s$ and $U^*_{Cr0} = U^*_{Cr0} / U_s$ get:

$$q = \frac{U^*_{Cr0} \left(1 - \Theta^n \right) + \left(1 - \Theta^{n_{Fr}} + 2 \sum_{i=1}^{n_{Fr}} \Theta^i \right) \Theta^{n_{Ds}}}{\left(1 - \Theta^{n_{Fr}} + 2 \sum_{i=1}^{n_{Fr}} \Theta^i \right) \Theta^{n_{Ds}} + \left(1 - \Theta^{n_{Ds}} + 2 \sum_{i=1}^{n_{Ds}} \Theta^i \right)}. \quad (2)$$

In the case of losses absence ($\Theta = 1$) equation (2) transforms in

$$q = \frac{n_{Fr}}{n}.$$

According to (2), the output voltage of the SRC does not depend on the load current and is determined only by the number of half-periods of resonant oscillations in the conversion phases.

For some values of the load resistance, oscillations in the circuit may end before the *Ds* or *Rv* conversion phase is complete. The condition for stopping oscillations in the circuit during the *Ds* or *Rv* transformation phase during the *k*-th pulse is equality $U_{Cr\text{k}} = U_{Ds}$ or $U_{Cr\text{k}} = U_{Rv}$ respectively. The time diagram of the resonant current for the zone of discontinuous currents is shown in fig. 5. The operation of the SRC in the zone of discontinuous currents leads to an increase in the level of output voltage ripples.

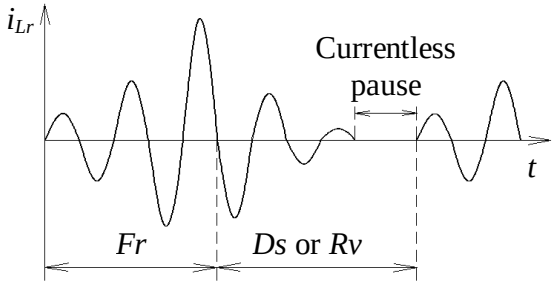

Fig. 5. Time diagram of resonant current for the zone of intermittent currents

It should be noted that under the same conditions, the amplitude of the resonant current in the *Rv* transformation phase decreases faster than in the *Ds* transformation phase. This is due to the fact that in the *Rv* conversion phase, energy is transferred not only to the load (as in the *Ds* conversion phase), but also to the input power source. Thus, with an increase in the total number of half-periods of resonant oscillations and in the case of using the *Rv* conversion phase, the zone of discontinuous currents increases.

The generalized SRC circuit is presented in fig. 6. The circuit consists of a direct voltage source at the input of the converter U_s, transistor M1 and diode M2 bridges, a series resonant circuit with the generalized resistance R_r, which characterizes the static and dynamic energy losses in the storage and switching elements of the inverter, the output capacitive filter and the load resistance R_{out}. The losses caused by the imperfection of the output filter are represented by the resistance R_f.

To build a mathematical model, it is convenient to use the state variable space method. The input is the source voltage U_s. The controlling influence is the number of pulses n_{Fr} and n_{Ds} (or n_{Rv}) per conversion cycle

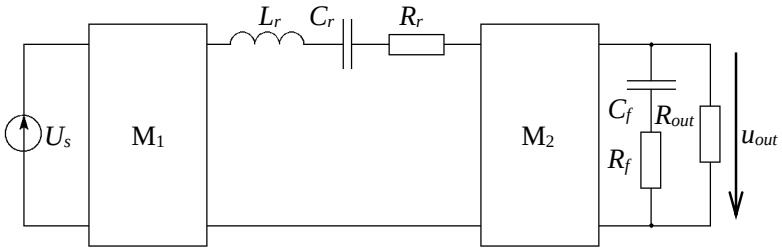

Fig. 6. Generalized SRC circuit

The output value is the the load voltage $y(t) = u_{out}(t)$. The processes occurring in the resonant circuit are characterized by the state vector – $\mathbf{x}^T(t) = [\ i_{Lr}(t)\ \ u_{Cr}(t)\ \ u_{Cf}(t)\ ]$.

To describe the electromagnetic processes of the SRC, it is necessary to draw up differential equations for each phase of the transformation. In addition, it is necessary to consider differential equations for the stage of the absence of oscillations in the zone of discontinuous currents.

Consider the transformation phase *Fr*. In this case, the switching bridges provide the resonant circuit voltage, which is equal to $U_s - u_{out}(t)$. Fig. 7 shows the equivalent circuits of the SRC in the *Fr* transformation phase (fig. 7, a – for the positive half-wave of the resonant current, fig. 7, b – for the negative half-wave).

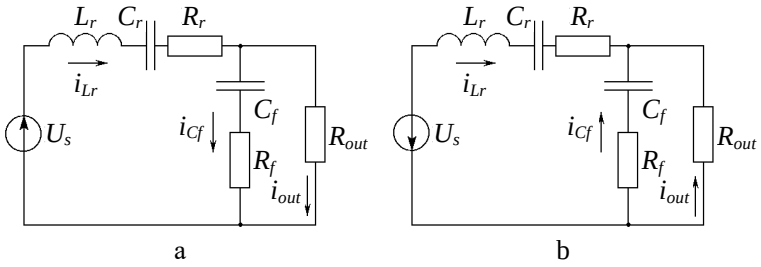

Fig. 7. Equivalent circuits of the PRP in the conversion phase *Fr*

Differential equations for the positive resonant current half-wave in the transformation phase *Fr* before and after transformation:

$$\begin{cases} L_r \cdot \dfrac{di_{Lr}}{dt} + i_{Lr} \cdot R_r + u_{Cr} + i_{Cf} \cdot R_f + \\ + u_{Cf} = U_s; \\ i_{Cf} \cdot R_f + u_{Cr} = \left(i_{Lr} - i_{Cf}\right) \cdot R_{out}; \\ C_r \cdot \dfrac{du_{Cr}}{dt} = i_{Lr}; \\ C_f \cdot \dfrac{du_{Cf}}{dt} = i_{Cf}; \\ u_{out} = u_{Cf} + i_{Cf} \cdot R_f. \end{cases} \quad (3)$$

$$\begin{cases} \dfrac{di_{Lr}}{dt} = -\dfrac{1}{L_r} \cdot \left(\dfrac{R_{out} \cdot R_f}{R_{out} + R_f} + R_r \right) \cdot i_{Lr} - \dfrac{1}{L_r} \cdot u_{Cr} - \\ - \dfrac{1}{L_r} \cdot \dfrac{R_{out}}{R_{out} + R_f} \cdot u_{Cf} + \dfrac{1}{L_r} \cdot U_s; \\ \dfrac{du_{Cr}}{dt} = \dfrac{1}{C_r} \cdot i_{Lr}; \\ \dfrac{du_{Cf}}{dt} = \dfrac{1}{C_f} \cdot \dfrac{R_{out}}{R_{out} + R_f} \cdot i_{Lr} - \dfrac{1}{C_f} \cdot \dfrac{1}{R_{out} + R_f} \cdot u_{Cf}; \\ u_{out} = \dfrac{R_{out} \cdot R_f}{R_{out} + R_f} \cdot i_{Lr} + \dfrac{R_{out}}{R_{out} + R_f} \cdot u_{Cf}. \end{cases} \quad (4)$$

Differential equations for the negative resonant current half-wave in the transformation phase *Fr* before and after transformation:

$$\begin{cases} L_r \cdot \dfrac{di_{Lr}}{dt} + i_{Lr} \cdot R_r + u_{Cr} - i_{Cf} \cdot R_f - \\ -u_{Cf} = -U_s; \\ i_{Cf} \cdot R_f + u_{Cf} = -\left(i_{Lr} - i_{Cf}\right) \cdot R_{out}; \\ C_r \cdot \dfrac{du_{Cr}}{dt} = i_{Lr}; \\ C_f \cdot \dfrac{du_{Cf}}{dt} = i_{Cf}; \\ u_{out} = u_{Cf} + i_{Cf} \cdot R_f. \end{cases} \quad (5)$$

$$\begin{cases} \dfrac{di_{Lr}}{dt} = -\dfrac{1}{L_r} \cdot \left(\dfrac{R_{out} \cdot R_f}{R_{out} + R_f} + R_r \right) \cdot i_{Lr} - \dfrac{1}{L_r} \cdot u_{Cr} + \\ + \dfrac{1}{L_r} \cdot \dfrac{R_{out}}{R_{out} + R_f} \cdot u_{Cf} - \dfrac{1}{L_r} \cdot U_s; \\ \dfrac{du_{Cr}}{dt} = \dfrac{1}{C_r} \cdot i_{Lr}; \\ \dfrac{du_{Cf}}{dt} = \dfrac{1}{C_f} \cdot \dfrac{R_{out}}{R_{out} + R_f} \cdot i_{Lr} - \dfrac{1}{C_f} \cdot \dfrac{1}{R_{out} + R_f} \cdot u_{Cf}; \\ u_{out} = -\dfrac{R_{out} \cdot R_f}{R_{out} + R_f} \cdot i_{Lr} + \dfrac{R_{out}}{R_{out} + R_f} \cdot u_{Cf}. \end{cases} \quad (6)$$

Consider the transformation phase *Ds*. In this case, the switching bridges provide a voltage on the resonant circuit, which is equal to $-u_{out}(t)$. Fig. 8 shows the equivalent circuits of the SRC in the *Ds* conversion phase (fig. 8, a – for the positive half-wave of the resonant current, fig. 8, b – for the negative half-wave).

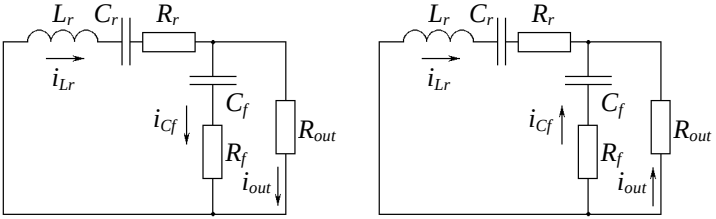

Fig. 8. Equivalent circuits of the SRC in the *Ds* conversion phase

Differential equations for the positive half-wave of the resonant current of the conversion phase *Ds* before and after the conversion:

$$\begin{cases} L_r \cdot \dfrac{di_{Lr}}{dt} + i_{Lr} \cdot R_r + u_{Cr} + i_{Cf} \cdot R_f + \\ + u_{Cf} = 0; \\ i_{Cf} \cdot R_f + u_{Cf} = \left(i_{Lr} - i_{Cf}\right) \cdot R_{out}; \\ C_r \cdot \dfrac{du_{Cr}}{dt} = i_{Lr}; \\ C_f \cdot \dfrac{du_{Cf}}{dt} = i_{Cf}; \\ u_{out} = u_{Cf} + i_{Cf} \cdot R_f. \end{cases} \quad (7)$$

$$\begin{cases} \dfrac{di_{Lr}}{dt} = -\dfrac{1}{L_r} \cdot \left(\dfrac{R_{out} \cdot R_f}{R_{out} + R_f} + R_r \right) \cdot i_{Lr} - \dfrac{1}{L_r} \cdot u_{Cr} - \\ - \dfrac{1}{L_r} \cdot \dfrac{R_{out}}{R_{out} + R_f} \cdot u_{Cf}; \\ \dfrac{du_{Cr}}{dt} = \dfrac{1}{C_r} \cdot i_{Lr}; \\ \dfrac{du_{Cf}}{dt} = \dfrac{1}{C_f} \cdot \dfrac{R_{out}}{R_{out} + R_f} \cdot i_{Lr} - \dfrac{1}{C_f} \cdot \dfrac{1}{R_{out} + R_f} \cdot u_{Cf}; \\ u_{out} = \dfrac{R_{out} \cdot R_f}{R_{out} + R_f} \cdot i_{Lr} + \dfrac{R_{out}}{R_{out} + R_f} \cdot u_{Cf}. \end{cases} \quad (8)$$

Differential equations for the negative half-wave of the resonant current of the conversion phase *Ds* before and after the conversion:

$$\begin{cases} L_r \cdot \dfrac{di_{Lr}}{dt} + i_{Lr} \cdot R_r + u_{Cr} - i_{Cf} \cdot R_f - u_{Cf} = 0; \\ i_{Cf} \cdot R_f + u_{Cf} = -\left(i_{Lr} - i_{Cf}\right) \cdot R_{out}; \\ C_r \cdot \dfrac{du_{Cr}}{dt} = i_{Lr}; \\ C_f \cdot \dfrac{du_{Cf}}{dt} = i_{Cf}; \\ u_{out} = u_{Cf} + i_{Cf} \cdot R_f. \end{cases} \quad (9)$$

$$\begin{cases} \dfrac{di_{Lr}}{dt} = -\dfrac{1}{L_r} \cdot \left(\dfrac{R_{out} \cdot R_f}{R_{out} + R_f} + R_r \right) \cdot i_{Lr} - \dfrac{1}{L_r} \cdot u_{Cr} + \\ + \dfrac{1}{L_r} \cdot \dfrac{R_{out}}{R_{out} + R_f} \cdot u_{Cf}; \\ \dfrac{du_{Cr}}{dt} = \dfrac{1}{C_r} \cdot i_{Lr}; \\ \dfrac{du_{Cf}}{dt} = \dfrac{1}{C_f} \cdot \dfrac{R_{out}}{R_{out} + R_f} \cdot i_{Lr} - \dfrac{1}{C_f} \cdot \dfrac{1}{R_{out} + R_f} \cdot u_{Cf}; \\ u_{out} = -\dfrac{R_{out} \cdot R_f}{R_{out} + R_f} \cdot i_{Lr} + \dfrac{R_{out}}{R_{out} + R_f} \cdot u_{Cf}. \end{cases} \quad (10)$$

Consider the *Rv* transformation phase. In this case, the switching bridges provide a voltage on the resonant circuit, which is equal to $-U_s - u_{out}(t)$. Fig. 9 shows the equivalent circuits of the SRC in the *Rv* conversion phase (fig. 9, a – for the positive half-wave of the resonant current, fig. 9, b – for negative).

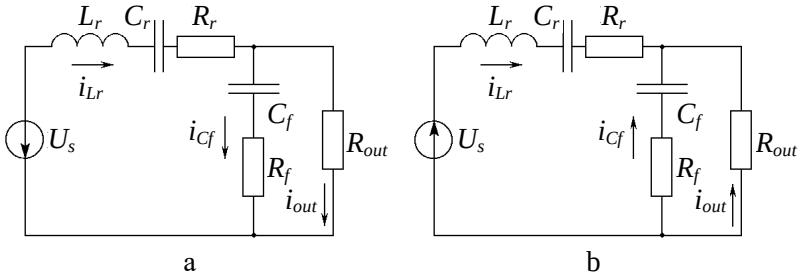

Fig. 9. Equivalent circuits of the SRC in the *Rv* conversion phase

Differential equations for the resonant current positive half-wave in the transformation phase *Rv* before and after transformation:

$$\begin{cases} L_r \cdot \dfrac{di_{Lr}}{dt} + i_{Lr} \cdot R_r + u_{Cr} + i_{Cf} \cdot R_f + \\ + u_{Cf} = -U_s; \\ i_{Cf} \cdot R_f + u_{Cf} = \left(i_{Lr} - i_{Cf}\right) \cdot R_{out}; \\ C_r \cdot \dfrac{du_{Cr}}{dt} = i_{Lr}; \\ C_f \cdot \dfrac{du_{Cf}}{dt} = i_{Cf}; \\ u_{out} = u_{Cf} + i_{Cf} \cdot R_f. \end{cases} \quad (11)$$

$$\begin{cases} \dfrac{di_{Lr}}{dt} = -\dfrac{1}{L_r} \cdot \left(\dfrac{R_{out} \cdot R_f}{R_{out} + R_f} + R_r \right) \cdot i_{Lr} - \dfrac{1}{L_r} \cdot u_{Cr} - \\ - \dfrac{1}{L_r} \cdot \dfrac{R_{out}}{R_{out} + R_f} \cdot u_{Cf} - \dfrac{1}{L_r} \cdot U_s; \\ \dfrac{du_{Cr}}{dt} = \dfrac{1}{C_r} \cdot i_{Lr}; \\ \dfrac{du_{Cf}}{dt} = \dfrac{1}{C_f} \cdot \dfrac{R_{out}}{R_{out} + R_f} \cdot i_{Lr} - \dfrac{1}{C_f} \cdot \dfrac{1}{R_{out} + R_f} \cdot u_{Cf}; \\ u_{out} = \dfrac{R_{out} \cdot R_f}{R_{out} + R_f} \cdot i_{Lr} + \dfrac{R_{out}}{R_{out} + R_f} \cdot u_{Cf}. \end{cases} \quad (12)$$

Differential equations for the resonant current negative half-wave in the transformation phase *Rv* before and after transformation:

$$\begin{cases} L_r \cdot \dfrac{di_{Lr}}{dt} + i_{Lr} \cdot R_r + u_{Cr} - i_{Cf} \cdot R_f - \\ -u_{Cf} = U_s; \\ i_{Cf} \cdot R_f + u_{Cf} = -\left(i_{Lr} - i_{Cf}\right) \cdot R_{out}; \\ C_r \cdot \dfrac{du_{Cr}}{dt} = i_{Lr}; \\ C_f \cdot \dfrac{du_{Cf}}{dt} = i_{Cf}; \\ u_{out} = u_{Cf} + i_{Cf} \cdot R_f. \end{cases} \quad (13)$$

$$\begin{cases} \dfrac{di_{Lr}}{dt} = -\dfrac{1}{L_r} \cdot \left(\dfrac{R_{out} \cdot R_f}{R_{out} + R_f} + R_r \right) \cdot i_{Lr} - \dfrac{1}{L_r} \cdot u_{Cr} + \\ + \dfrac{1}{L_r} \cdot \dfrac{R_{out}}{R_{out} + R_f} \cdot u_{Cf} + \dfrac{1}{L_r} \cdot U_s; \\ \dfrac{du_{Cr}}{dt} = \dfrac{1}{C_r} \cdot i_{Lr}; \\ \dfrac{du_{Cf}}{dt} = \dfrac{1}{C_f} \cdot \dfrac{R_{out}}{R_{out} + R_f} \cdot i_{Lr} - \dfrac{1}{C_f} \cdot \dfrac{1}{R_{out} + R_f} \cdot u_{Cf}; \\ u_{out} = -\dfrac{R_{out} \cdot R_f}{R_{out} + R_f} \cdot i_{Lr} + \dfrac{R_{out}}{R_{out} + R_f} \cdot u_{Cf}. \end{cases} \quad (14)$$

Consider the stage of absence of resonant oscillations during the *Ds* or *Rv* conversion phases. In this case, the resonant circuit is disconnected from the power source and the load. The capacity of the filter is discharged by load. The equivalent SRC circuit for the stage of absence of resonant oscillations is shown in Fig. 10. The expressions describing electromagnetic processes in the diagram in Fig. 10:

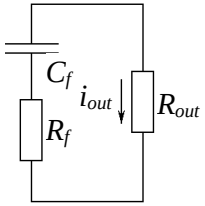

Fig. 10. Equivalent circuit of the SRC for the stage of absence of resonant oscillations

$$\begin{cases} \dfrac{du_{Cf}}{dt} = \dfrac{u_{Cf}}{(R_f + R_{out})C_f}; \\ u_{out} = \dfrac{R_{out}}{R_{out} + R_f} \cdot u_{Cf}. \end{cases} \quad (15)$$

Systems of equations (4), (6), (8), (10), (12), (14) and (15) in matrix form:

a) for the conversion phase *Fr* (at the positive half-wave of the resonant current)

$$\dot{\mathbf{x}}(t) = \mathbf{A}_1 \cdot \mathbf{x}(t) + \mathbf{b}_1 \cdot U_s; \quad (16)$$

$$y(t) = \mathbf{C}_1 \cdot \mathbf{x}(t); \quad (17)$$

b) for the conversion phase *Fr* (at the negative half-wave of the resonant current)

$$\dot{\mathbf{x}}(t) = \mathbf{A}_2 \cdot \mathbf{x}(t) + \mathbf{b}_2 \cdot U_s; \quad (18)$$

$$y(t) = \mathbf{C}_2 \cdot \mathbf{x}(t); \quad (19)$$

c) for the conversion phase *Ds* (at the positive half-wave of the resonant current)

$$\dot{\mathbf{x}}(t) = \mathbf{A}_1 \cdot \mathbf{x}(t) + \mathbf{b}_3 \cdot U_s ; \quad (20)$$

$$y(t) = \mathbf{C}_1 \cdot \mathbf{x}(t) ; \quad (21)$$

d) for the conversion phase *Ds* (at the negative half-wave of the resonant current)

$$\dot{\mathbf{x}}(t) = \mathbf{A}_2 \cdot \mathbf{x}(t) + \mathbf{b}_3 \cdot U_s ; \quad (22)$$

$$y(t) = \mathbf{C}_2 \cdot \mathbf{x}(t) ; \quad (23)$$

e) for the conversion phase *Rv* (at the positive half-wave of the resonant current)

$$\dot{\mathbf{x}}(t) = \mathbf{A}_1 \cdot \mathbf{x}(t) + \mathbf{b}_2 \cdot U_s ; \quad (24)$$

$$y(t) = \mathbf{C}_1 \cdot \mathbf{x}(t) ; \quad (25)$$

f) for the conversion phase *Rv* (at the negative half-wave of the resonant current)

$$\dot{\mathbf{x}}(t) = \mathbf{A}_2 \cdot \mathbf{x}(t) + \mathbf{b}_1 \cdot U_s ; \quad (26)$$

$$y(t) = \mathbf{C}_2 \cdot \mathbf{x}(t) ; \quad (27)$$

g) at the absence of oscillations in the circuit

$$\dot{\mathbf{x}}(t) = \mathbf{A}_3 \cdot \mathbf{x}(t) + \mathbf{b}_3 \cdot U_s ; \quad (28)$$

$$y(t) = \mathbf{C}_3 \cdot \mathbf{x}(t) , \quad (29)$$

where

$$\mathbf{A}_3 = \begin{bmatrix} 0 & 0 & 0 \\ 0 & 0 & 0 \\ 0 & 0 & \dfrac{1}{C_f (R_{out} + R_f)} \end{bmatrix}; \ \mathbf{b}_1 = \begin{bmatrix} \dfrac{1}{L_r} \\ 0 \\ 0 \end{bmatrix}; \ \mathbf{b}_2 = \begin{bmatrix} -\dfrac{1}{L_r} \\ 0 \\ 0 \end{bmatrix}; \ \mathbf{b}_3 = 0 ;$$

$$\mathbf{C}_1 = \begin{bmatrix} \dfrac{R_{out} R_f}{R_{out} + R_f} & 0 & \dfrac{R_{out}}{R_{out} + R_f} \end{bmatrix}; \ \mathbf{C}_2 = \begin{bmatrix} -\dfrac{R_{out} R_f}{R_{out} + R_f} & 0 & \dfrac{R_{out}}{R_{out} + R_f} \end{bmatrix};$$

$$\mathbf{C}_3 = \begin{bmatrix} 0 & 0 & \dfrac{R_{out}}{R_{out} + R_f} \end{bmatrix}.$$

$$\mathbf{A}_1 = \begin{bmatrix} -\frac{1}{L_r}\left(\frac{R_{out}R_f}{R_{out}+R_f}+R_r\right) & -\frac{1}{L_r} & -\frac{R_{out}}{L_r(R_{out}+R_f)} \\ \frac{1}{C_r} & 0 & 0 \\ \frac{R_{out}}{C_f(R_{out}+R_f)} & 0 & -\frac{1}{C_f(R_{out}+R_f)} \end{bmatrix};$$

$$\mathbf{A}_2 = \begin{bmatrix} -\frac{1}{L_r}\left(\frac{R_{out}R_f}{R_{out}+R_f}+R_r\right) & -\frac{1}{L_r} & \frac{R_{out}}{L_r(R_{out}+R_f)} \\ \frac{1}{C_r} & 0 & 0 \\ -\frac{R_{out}}{C_f(R_{out}+R_f)} & 0 & -\frac{1}{C_f(R_{out}+R_f)} \end{bmatrix};$$

Matrixes $\mathbf{A}_1$, $\mathbf{A}_2$, $\mathbf{A}_3$ describe the topology of the circle, matrixes $\mathbf{b}_1$, $\mathbf{b}_2$, $\mathbf{b}_3$ – connecting the input voltage source, the matrixes $\mathbf{C}_1$, $\mathbf{C}_2$, $\mathbf{C}_3$ – load connection. The solution of differential equations (16), (18), (20), (22), (24), (4.26), (28) are the functions:

a) for the conversion phase *Fr* (at the positive half-wave of the resonant current)

$$\mathbf{x}(t) = e^{\mathbf{A}_1 \cdot t} \cdot \mathbf{x}\left(kT_r\right) + \mathbf{D}_1(t) \cdot \mathbf{b}_1 \cdot U_s\,, \tag{30}$$

where k – the number of entire periods of resonance oscillations that have passed since the beginning of the transformation phase;

b) for the conversion phase *Fr* (at the negative half-wave of the resonant current)

$$\mathbf{x}(t) = e^{\mathbf{A}_2 \cdot t} \cdot \mathbf{x}\left(\left(k+\frac{1}{2}\right)T_r\right) + \mathbf{D}_2(t) \cdot \mathbf{b}_2 \cdot U_s\,; \tag{31}$$

c) for the conversion phase *Ds* (at the positive half-wave of the resonant current)

$$\mathbf{x}(t) = e^{\mathbf{A}_1 \cdot t} \cdot \mathbf{x}\left(kT_r\right); \tag{32}$$

d) for the conversion phase *Ds* (at the negative half-wave of the resonant current)

$$\mathbf{x}(t) = e^{\mathbf{A}_2 \cdot t} \cdot \mathbf{x}\left(\left(k+\frac{1}{2}\right)T_r\right); \tag{33}$$

e) for the conversion phase *Rv* (at the positive half-wave of the resonant current)

$$\mathbf{x}(t) = e^{\mathbf{A}_1 \cdot t} \cdot \mathbf{x}\left(kT_r\right) + \mathbf{D}_1(t) \cdot \mathbf{b}_2 \cdot U_s; \quad (34)$$

f) for the conversion phase *Rv* (at the negative half-wave of the resonant current)

$$\mathbf{x}(t) = e^{\mathbf{A}_2 \cdot t} \cdot \mathbf{x}\left(\left(k + \frac{1}{2}\right)T_r\right) + \mathbf{D}_2(t) \cdot \mathbf{b}_1 \cdot U_s; \quad (35)$$

g) at the absence of oscillations in the circuit

$$\mathbf{x}(t) = e^{\mathbf{A}_3 \cdot t} \cdot \mathbf{x}\left(kT_r\right), \quad (36)$$

where

$$\mathbf{D}_1(t) = \int_0^t e^{\mathbf{A}_1 \cdot (t-\tau)} \cdot d\tau = \mathbf{A}_1^{-1} \cdot \left(e^{A_1 \cdot t} - \mathbf{I}\right);$$

$$\mathbf{D}_2(t) = \int_0^t e^{\mathbf{A}_2 \cdot (t-\tau)} \cdot d\tau = \mathbf{A}_2^{-1} \cdot \left(e^{A_2 \cdot t} - \mathbf{I}\right);$$

I – unit diagonal matrix.

Expressions (17), (19), (21), (23), (25), (27), (29), (30) (36) allow to study the processes in the power section of the SRC for possible PhC and different modes of operation. The operating mode of the SRC depends on the load parameters and the amount of energy accumulated in the resonant circuit. As a result, to describe the dynamic processes in the power part of the converter, it is necessary to carry out numerical modeling of electromagnetic processes in the SRC. For this, it is convenient to use expressions (17), (19), (21), (23), (25), (27), (29), (30) (36), taking into account the specific PhC and the presence of the continuous resonant current regime outline.

The operation of the SRC in the zone of continuous currents consists of two stages: a) direct transfer of energy from the source to the load and resonant circuit (phase of conversion *Fr*); b) dissipation of the energy accumulated in the resonant circuit to the load (transformation phase *Ds*). The transformation cycle consists of n_{Fr} half-periods of resonant oscillations of the transformation phase *Fr* and n_{Ds} half-periods of the transformation phase *Ds* (the duration of each half-period – $T_r/2$). Total number of half periods $n = n_{Fr} + n_{Ds}$.

Using (30) and (31), the state vector after n_{Fr} half-periods of the *Fr* conversion phase is obtained:

$$\mathbf{x}\left(n_{Fr}\frac{T_r}{2}\right)=\mathbf{A}_{Fr}\mathbf{x}(0)+\mathbf{B}_{Fr}U_s, \tag{37}$$

where $\mathbf{x}(0)$ – value of the state vector at the beginning of the conversion cycle;

$$\mathbf{A}_{Fr}=e^{\left[\left(2n_{Fr}+1-(-1)^{n_{Fr}}\right)\mathbf{A}_1+\left(2n_{Fr}-1+(-1)^{n_{Fr}}\right)\mathbf{A}_2\right]\frac{T_r}{8}};$$

$$\mathbf{B}_{Fr}=\left[\left(\sum_{i=0}^{m_1}e^{\left[\left(i-\frac{1+(-1)^{n_{Fr}}}{2}\right)\mathbf{A}_1+i\mathbf{A}_2\right]\frac{T_r}{2}}-\frac{1+(-1)^{n_{Fr}}}{2}e^{-\mathbf{A}_1\frac{T_r}{2}}\right)\mathbf{D}_1\left(\frac{T_r}{2}\right)-\right.$$

$$\left.\left(\sum_{i=0}^{m_2}e^{\left[\left(i-\frac{1-(-1)^{n_{Fr}}}{2}\right)\mathbf{A}_2+i\mathbf{A}_1\right]\frac{T_r}{2}}-\frac{1-(-1)^{n_{Fr}}}{2}e^{-\mathbf{A}_2\frac{T_r}{2}}\right)\mathbf{D}_2\left(\frac{T_r}{2}\right)\right]\mathbf{b};$$

$$m_1=\frac{2n_{Fr}-1+(-1)^{n_{Fr}}}{4};\ m_2=\frac{2n_{Fr}-3-(-1)^{n_{Fr}}}{4};\ \mathbf{b}=\mathbf{b}_1=-\mathbf{b}_2.$$

Using (32), (33) and (37), the state vector after n_{Ds} half-periods of the conversion phase *Ds* is obtained:

$$\mathbf{x}\left(n\frac{T}{2}\right)=\mathbf{A}_{Ds}\mathbf{x}\left(n_{Fr}\frac{T_r}{2}\right)=\mathbf{A}_{Ds}\left[\mathbf{A}_{Fr}\mathbf{x}(0)+\mathbf{B}_{Fr}U_s\right], \tag{38}$$

where $\mathbf{A}_{Ds}=e^{\left[\left(2n_{Ds}+1-(-1)^{n_{Ds}}\right)\mathbf{A}_2+\left(2n_{Ds}-1+(-1)^{n_{Ds}}\right)\mathbf{A}_1\right]\frac{T_r}{8}}$.

To obtain the transfer function for small disturbances of the input voltage, it is necessary to consider the disturbance of the input voltage:

$$U_s(t)=U_s+u_s^*(t), \tag{39}$$

where $u_s^*(t)$ – disturbance of the input voltage.

In the presence of disturbances in the input voltage (39) taking into account (38) and (17), it is possible to write:

$$\underline{\mathbf{x}}\left(n\frac{T_r}{2}\right)+\mathbf{x}^*\left(n\frac{T_r}{2}\right)=\mathbf{A}_{Ds}\left[\mathbf{A}_{Fr}\left(\underline{\mathbf{x}}(0)+\mathbf{x}^*(0)\right)+\mathbf{B}_{Fr}\left(U_s+u_s^*(0)\right)\right] \tag{40}$$

;

$$\underline{y}(0)+y^*(0)=\mathbf{C}_1\left(\underline{\mathbf{x}}(0)+\mathbf{x}^*(0)\right), \tag{41}$$

where $\underline{\mathbf{x}}$ and $\underline{y}$ – average values of the state vector and the output voltage; $\mathbf{x}^*$ and y^* disturbance of the state vector and the output voltage.

After the transformation of (40) and (41), the expressions of the disturbances of the state vector and the output voltage are

$$\mathbf{x}^*\left(n\frac{T_r}{2}\right) = \mathbf{A}_{Ds}\left[\mathbf{A}_{Fr}\mathbf{x}^*(0) + \mathbf{B}_{Fr}u_s^*(0)\right]; \tag{42}$$

$$y^*(0) = \mathbf{C}_1\mathbf{x}^*(0). \tag{43}$$

After transforming (42) and (43) into the continuous form:

$$\mathbf{x}^*\left(t + n\frac{T_r}{2}\right) = \mathbf{A}_{Ds}\left[\mathbf{A}_{Fr}\mathbf{x}^*(t) + \mathbf{B}_{Fr}u_s^*(t)\right]; \tag{44}$$

$$y^*(t) = \mathbf{C}_1\mathbf{x}^*(t). \tag{45}$$

After transforming (44) and (45) into the operator form:

$$\mathbf{I}e^{n\frac{T_r}{2}p}\mathbf{x}^*(p) = \mathbf{A}_{Ds}\left[\mathbf{A}_{Fr}\mathbf{x}^*(p) + \mathbf{B}_{Fr}u_s^*(p)\right]; \tag{46}$$

$$y^*(p) = \mathbf{C}_1\mathbf{x}^*(p). \tag{47}$$

Using (47), the state vector disturbance $\mathbf{x}^*(p)$ to disturbance of the input voltage $u_s^*(p)$ ratio is obtained:

$$W_x(p) = \frac{\mathbf{x}^*(p)}{u_s^*(p)} = \mathbf{A}_{Ds}\mathbf{B}_{Fr}\left[\mathbf{I}e^{n\frac{T_r}{2}p} - \mathbf{A}_{Ds}\mathbf{A}_{Fr}\right]^{-1}. \tag{48}$$

From (48) the transfer function of the converter $W_U(p)$ is obtained:

$$W_U(p) = \frac{y^*(p)}{u_s^*(p)} = \mathbf{C}_1\frac{\mathbf{x}^*(p)}{u_s^*(p)}. \tag{49}$$

Using (48) and (49), the transfer function for small perturbations of the input voltage for the zone of continuous currents is obtained:

$$W_U(p) = \mathbf{C}_1\mathbf{A}_{Ds}\mathbf{B}_{Fr}\left[\mathbf{I}e^{n\frac{T_r}{2}p} - \mathbf{A}_{Ds}\mathbf{A}_{Fr}\right]^{-1}. \tag{50}$$

Thus, the obtained mathematical model of the SRC with pulse-number regulation allows to build static characteristics and to study the processes in the power part of the SRC for the mode of continuous currents. Expression (50), which describes the transfer function for small disturbances in the input voltage, can be used to estimate their effect on the output voltage of the converter.

The operation of the SRC in the zone of discontinuous currents consists of three stages: a) direct transfer of energy from the source to the load and resonant circuit (phase of conversion *Fr*); b) dissipation of the energy accumulated in the resonant circuit to the load (transformation phase *Ds*);

c) oscillationstopping in the resonant circuit and dissipation of the energy accumulated in the filter capacity to the load.

The conversion cycle consists of n_{Fr} half-periods of the *Fr* conversion phase and n_{Ds} half-periods of the *Ds* conversion phase (oscillations in the circuit disappear after n_{Ds1} half-periods of the *Ds* conversion phase). Total number of half periods is $n = n_{Fr} + n_{Ds}$.

The expression for the state vector after n_{Fr} half-periods of the transformation phase *Fr* can be found similarly to (37). According to (32) and (33), the state vector after n_{Ds1} half-periods of the conversion phase *Ds* is

$$\mathbf{x}\left(\left(n_{Fr}+n_{Ds1}\right)\frac{T_r}{2}\right)=\mathbf{A}_{Ds}\mathbf{x}\left(n_{Fr}\frac{T_r}{2}\right)=\mathbf{A}_{Ds1}\left[\mathbf{A}_{Fr}\mathbf{x}(0)+\mathbf{B}_{Fr}U_s\right], \quad (51)$$

where $\mathbf{A}_{Ds1}=e^{\left[\left(2n_{Ds1}+1-(-1)^{nDs1}\right)\mathbf{A}_2+\left(2n_{Ds1}-1+(-1)^{nDs1}\right)\mathbf{A}_1\right]\frac{T_r}{8}}$.

According to (36) and (51), the state vector after n_{Ds} half-periods of the conversion phase *Ds*:

$$\begin{aligned}\mathbf{x}\left(n\frac{T_r}{2}\right)&=\mathbf{A}_{Ds2}\mathbf{x}\left(\left(n_{Fr}+n_{Ds1}\right)\frac{T_r}{2}\right)=\\&=\mathbf{A}_{Ds2}\mathbf{A}_{Ds1}\left[\mathbf{A}_{Fr}\mathbf{x}(0)+\mathbf{B}_{Fr}U_s\right],\end{aligned} \quad (52)$$

where $\mathbf{A}_{Ds2}=e^{\left(2n_{Ds2}+1-(-1)^{nDs2}\right)\mathbf{A}_3\frac{T_r}{8}}$; $n_{Ds2}=n_{Ds}-n_{Ds1}$.

In the presence of disturbances in the input voltage, taking into account (39) and (52), it is possible to write:

$$\underline{\mathbf{x}}\left(n\frac{T_r}{2}\right)+\mathbf{x}^*\left(n\frac{T_r}{2}\right)=\mathbf{A}_{Ds2}\mathbf{A}_{Ds1}\left[\mathbf{A}_{Fr}\left(\underline{\mathbf{x}}(0)+\mathbf{x}^*(0)\right)+\mathbf{B}_{Fr}\left(U_s+u_s^*(0)\right)\right] \quad (53)$$

After transformation (53), the expression for disturbances of the state vector of the zone of intermittent currents is obtained:

$$\mathbf{x}^*\left(n\frac{T_r}{2}\right)=\mathbf{A}_{Ds2}\mathbf{A}_{Ds1}\left[\mathbf{A}_{Fr}\mathbf{x}^*(0)+\mathbf{B}_{Fr}u_s^*(0)\right]. \quad (54)$$

After transformation (54), the expression for disturbances of the state vector of the zone of discontinuous currents in a continuous form can be written as:

$$\mathbf{x}^*\left(t+n\frac{T_r}{2}\right)=\mathbf{A}_{Ds2}\mathbf{A}_{Ds1}\left[\mathbf{A}_{Fr}\mathbf{x}^*(t)+\mathbf{B}_{Fr}u_s^*(t)\right]. \quad (55)$$

The expression for disturbances of the state vector (55) of the zone of discontinuous currents in operator form can be written as:

$$\mathbf{I}e^{n\frac{T_r}{2}p}\mathbf{x}^*(p)=\mathbf{A}_{Ds2}\mathbf{A}_{Ds1}\left[\mathbf{A}_{Fr}\mathbf{x}^*(p)+\mathbf{B}_{Fr}u_s^*(p)\right]. \quad (56)$$

Using (56), the transfer function $W_x(p)$ for the zone of discontinuous currents is obtained:

$$W_x(p) = \frac{\mathbf{x}^*(p)}{u_s^*(p)} = \mathbf{A}_{Ds2}\mathbf{A}_{Ds1}\mathbf{B}_{Fr}\left[\mathbf{I}e^{n\frac{T_r}{2}p} - \mathbf{A}_{Ds2}\mathbf{A}_{Ds1}\mathbf{A}_{Fr}\right]^{-1}. \qquad (57)$$

Using (49) and (57) the transfer function for small disturbances of the input voltage of the discontinuous current zone is obtained:

$$W_U(p) = \mathbf{C}_1\mathbf{A}_{Ds2}\mathbf{A}_{Ds1}\mathbf{B}_{Fr}\left[\mathbf{I}e^{n\frac{T_r}{2}p} - \mathbf{A}_{Ds2}\mathbf{A}_{Ds1}\mathbf{A}_{Fr}\right]^{-1}. \qquad (58)$$

The mathematical model of the SRC with pulse-number control allows to obtain static characteristics and study electromagnetic processes in the power section of the SRC for the discontinuous current regime. Expression (58) describing the transfer function for small disturbances in the input voltage can be used to estimate their effect on the output voltage of the converter.

2. Static and dynamic characteristics of the DC-DC series resonant converter

It is advisable to use SRC mathematical models to obtain its static characteristics. In the zone of continuous currents, it is necessary to find a joint solution of equations (37) and (38), and in the zone of discontinuous currents – equations (37), (38), (51) and (52). The load current in relative units is determined by the expression

$$I_{out}^* = \frac{I_{out} \cdot \rho}{U_s}.$$

In fig. 11, a one can see the load characteristics of the series-resonant converter obtained with the total number of half-periods $n = 20$ and the number of half-periods of the conversion phase Fr $n_{Fr} = const$ taking into account the zone of intermittent currents, which is shown by a dashed line.

The voltage applied to the circuit in the Fr conversion phase approaches zero, as the corresponding output current does. At U_{out}, the voltage applied to the circuit in the Fr conversion phase approaches U_s, but the number of half-periods n_{Fr} of the conversion phase Fr is minimal and equal to 1. In these cases, the load current approaches the minimum value that depends on the ratio n_{Fr}/n and the load resistance. When $U_{out} = U_s/2$, the voltage applied to the circuit in the conversion phase Fr is $U_s/2$, and the number of half-cycles of the conversion phase Fr is half of the total number of half-cycles. Due to this, the load current increases. As a result, the width of the discontinuous currents zone is maximal in the region of $q =$

0.5, and minimal at $q = 0$ and $q = 1$. The values of load characteristics in the discontinuous currents zone approach $q = 1$. This is due to the fact that in the absence of *Ds* phase current pulses, all energy is transferred to the conversion phase *Fr*. And this is possible only when $U_{out} = U_s$.

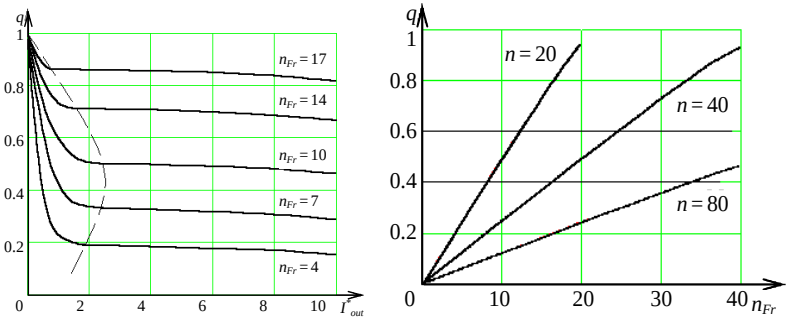

Fig. 11. Load and control characteristics of the SRC

Fig. 11, b shows control characteristics for SRC at $n_{Fr} = const$ for the continuous currents zone. The control characteristics for SRC in the area of continuous currents are practically linear, which simplifies the process of regulating the output voltage.

To ensure trouble-free operation of the SRC, it is necessary to determine the areas in which the values of the maximum resonant capacitor voltage $U_{Cr\,m}$ and the maximum resonant current $I_{Lr\,m}$ do not exceed the specified value. The maximum voltage and current values will occur at the end of the conversion phase *Fr*, since in this conversion phase the energy is stored in the resonant circuit, and in the conversion phases *Ds* and *Rv*, the energy of the resonant circuit is dissipated on the load or through the power source. When constructing isoparametric characteristics, relative units were used:

$$U^*_{Cr\,m} = \frac{U_{Cr\,m}}{U_s};\ I^*_{Lr\,m} = \frac{I_{Lr\,m} \cdot \rho}{U_s}.$$

Fig. 12, a shows isoparametric characteristics of SRC at $U^*_{Cr\,m} = const$, and fig.12, b – at $I^*_{Lr\,m} = const$. The solid line shows the characteristics at $n = 10$, the dashed line at $n = 20$. The boundaries of the discontinuous current zones at $n = 10$ and $n = 20$ are shown as well.

The values of the maximum voltage and current depend on the magnitude of the voltage applied to the resonant circuit and the number of half-periods of the conversion phase *Fr*. The largest amplitude values

occur at $U_{out} = U_s/2$, since the voltage applied to the resonant circuit is equal to $U_s/2$ and the number of half-periods of the conversion phase *Fr* is equal to the half of the total number of half-periods. As U_{out} approaches zero, the voltage applied to the resonant circuit is equal to U_s, but the number of half-periods of the conversion phase *Fr* is minimal. As U_{out} approaches U_s, the number of half-cycles of the conversion phase *Fr* is maximum, but the voltage applied to the circuit approaches zero. The zone of safe operation also depends on the total number of half-cycles. When the total number of half-periods increases, the conversion phase *Fr* number of half-periods increases, which leads to an increase in the maximum voltage and current values. In the zone of intermittent currents, the isoparametric characteristics shift to the left due to the end of the oscillations before the end of the conversion phase *Ds*, which causes a decrease in the load current.

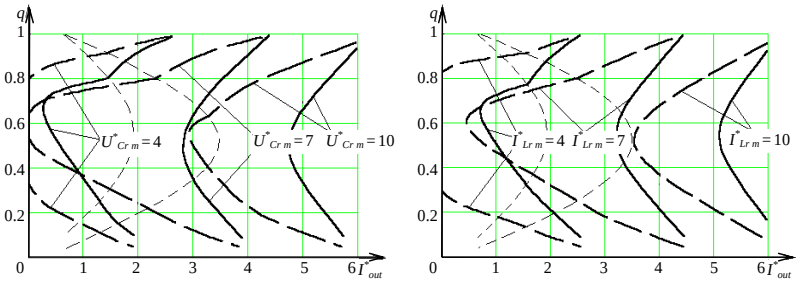

Fig. 12. Isoparametric characteristics of the SRC

In the discontinuous currents zone, the isoparametric characteristics shift to the left due to the disappearance of oscillations before the end of the *Rv* transformation phase, which causes a decrease in the load current. Isoparametric characteristics make it possible to determine the zone of safe operation of the SRC at the given maximum values of the voltage of the resonant capacitor and the resonant current.

Fig. 13, a shows the logarithmic frequency responses (LFR) of the SRC with the following circuit parameters: L_r = 128 μH, C_r = 19.8 nF, R_r = 1 Ohm, C_f = 1000 μF, R_f = 0.1 Ohm, R_{out} = 100 Ohm. The characteristics are built at $n_{Fr} = const$ and $n = 40$.

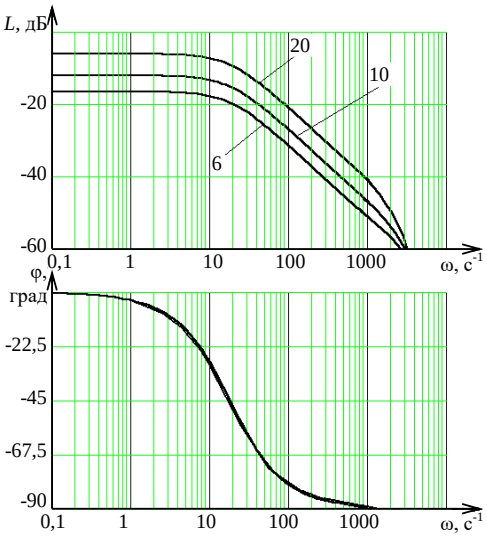

a

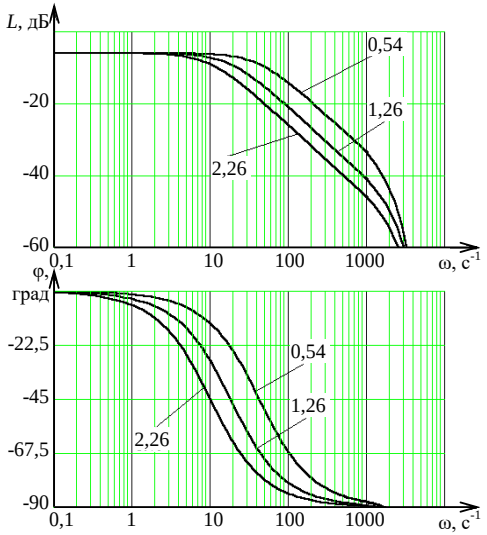

b

Fig. 13. Logarithmic frequency responses of the SRC at $n_{Fr} = const$ (a) and $R_{out} = const$ (b)

Fig. 13,b shows the logarithmic phase-frequency response (LPFR) of the SRC when the load resistance changes. The responses are constructed at $R_{out}/\rho = const$ and $n_{Fr} = 20$, $n = 40$. LPFR is obtained using (50). Their curves show that the transfer function of the SRC in the simplified form can be represented as a link with the time delay of $n_{Tr}/2$ and an aperiodic link with the load time constant.

3. Control system of resonant dc voltage converter with pulse-number regulation

The pulse-number control principle makes it possible to ensure linear adjustment and rigid load characteristics in resonance-type converters. However, the use of the resonant circuit in the converter leads to a significant increase in the instantaneous values of currents and voltages above the average values. To determine the maximum values of current and voltage in the resonant circuit, it is necessary to consider the phase *Fr*, during which energy is accumulated in the circuit and, accordingly, the resonant capacitor voltage increases. The resonant capacitor voltage reaches its maximum value at the end of the *Fr* phase and is determined by the number of pulses n_{Fr} in the *Fr* phase, the ratio of the input U_s and output U_{out} voltages, the value of the initial voltage resonant capacitor U_{Cr0}. With the pulse-number control, the output voltage can change with a certain step of discreteness. To reduce the discreteness step, it is necessary to increase the total number of pulses n per conversion cycle and, accordingly, the number of pulses n_{Fr} in the *Fr* phase. This leads to an increase in the resonant capacitor voltage, which is unacceptable because the maximum values of the resonant capacitor current and voltage exceed the permissible values.

The control discreteness step is inversely proportional to the total number of pulses n. At the same time, the maximum values of the voltage on the resonant capacitor and the current in the resonant circuit are proportional to this value. This problem can be solved by dividing the main conversion cycle into several small conversion cycles, which makes it possible to reduce the maximum values of the resonant capacitor voltage and the resonant circuit current.

For this purpose, the conversion cycle, which consists of $n = n_{Fr} + n_{Ds}$ pulses, is divided into several small cycles consisting of $n_i = n_{Fri} + n_{Dsi}$ pulses, where $i = 1..m$ is the number of the small conversion cycle. To describe the processes during such a replacement, the resonant circuit to which the inverter voltage U_{inv} is applied is considered. Time diagrams during one conversion cycle are shown in Fig. 14. To simplify

calculations, losses in the circuit are not taken into account. The expressions for the amplitude values of the resonant capacitor voltage and the resonant circuit current for the *k*-th pulse are determined by the dependencies:

$$U_{Crk} = (2k \cdot U_{inv} - U_{Cr0}) \cdot (-1)^{k+1};\ I_{Lrk} = \frac{(2k-1) \cdot U_{inv} - U_{Cr0}}{\rho}.$$

Each phase of the conversion contains a certain number of pulses, n_{Fr} and n_{Ds} respectively. Total number of pulses $n = n_{Fr} + n_{Ds}$ must be paired to ensure stability of operation.

The resonant capacitor voltage at the end of the conversion cycle:

$$U_{Crn} = [2 \cdot n_{Ds} \cdot U_{Ds} (-1)^{n_{Fr}} - (2 \cdot n_{Fr} \cdot U_{Fr} - U_{Cr0})(-1)^{n_{Fr}+1}] \cdot (-1)^{n_{Ds}+1}.$$

To ensure the energy balance, a condition $U_{Crn} = U_{Cr0}$ must be met. After the conversion obtain $n_{Fr}U_{Fr} + n_{Ds}U_{Ds} = 0$.

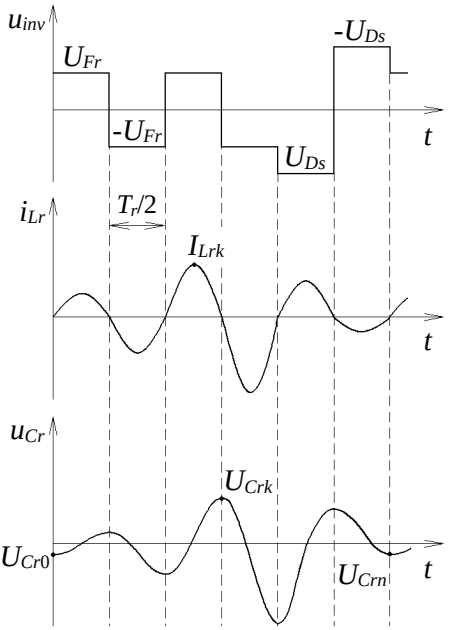

Fig. 14. Time diagrams for one conversion cycle

Taking into account the expressions for U_{Fr}, U_{Ds} and q receive:

$$q = \frac{n_{Fr}}{n}. \tag{59}$$

Taking into account the energy balance condition for m small periods, it can be proved that

$$q = \frac{\sum_{i=1}^{m} n_{Fr_i}}{\sum_{i=1}^{m} \left(n_{Fr_i} + n_{Ds_i} \right)}. \tag{60}$$

Comparing (59) and (60), it can be concluded that when matching $n_{Fr} = \sum_{i=1}^{m} n_{Fr_i}$ and $n_{Ds} = \sum_{i=1}^{m} n_{Ds_i}$ the main conversion cycle can be broken into several small cycles.

The resonant current and resonant capacitor voltage reach their maximum values at the end of the *Fr* phase. The maximum values depend on the ratio of the source and load voltages, the load current and the number of pulses of the phase *Fr*. When the main conversion cycle is divided into several small cycles, the maximum values of current and voltage in the resonant circuit will be determined by the number of n_{Fri} pulses in the Fr_i phase in one of the small cycles, which is significantly less than the total number of n_{Fr} pulses in the *Fr* phases for the complete conversion cycle.

Splitting the main conversion cycle into several small cycles leads to a decrease in the level of output voltage ripples with the period $(n_{Fr} + n_{Ds})T_r/2$ and the appearance of pulsations with the periods $(n_{Fri} + n_{Dsi})T_r/2$, which are more effectively reduced by the output filter. The size of the discontinuous currents zone depends on the total number of pulses of the conversion cycle. The introduction of small conversion cycles allows reducing the area of discontinuous currents.

Since the clocking of the SRC with pulse-number control depends on the presence of resonant current pulses, when working in the area of discontinuous currents, it is necessary to provide for the internal clocking of the control system in the event that resonant oscillations stop before the end of the control period. For this, the control system must measure the half-period of resonant oscillations at the beginning of the Fr_i phase and, when transitioning to the Ds_i phase, withstand the time interval $n_{Dsi}T_r/2$, and after the end of this interval, make a forced transition to the phase Fr_{i+1}.

Thus, the SRC control system with pulse-number control should solve the following tasks:

• determination of the number of pulses in each of the phases of operation in accordance with the required voltage level at the output of the SRC;

• limiting the maximum values of resonant current and voltage on the resonant capacitor;

• ensuring the stability of the SRC operation in the area of intermittent currents.

To solve the basic tasks of pulse-number control, a certain number of calculations must be performed. These calculations must be performed during the main conversion cycle. To build a control system, a wide range of inexpensive microcontrollers with a large number of peripheral modules is offered, which allow you to implement a control system with a minimum number of external elements.

Fig. 15 shows the functional control circuit of the SRC with pulse-number regulation. The circuit contains a microcontroller MC, a synchronization device SD, a peak detector PD and a current sensor CS.

MK pre-sets the control signal u_{contr} with the help of which the SD determines the phase of operation (*Fr* or *Ds*) and changes the control signal for the switches of the bridge M1 when the polarity of the resonant current changes. The control influence is changed by the u_{sync} signal, which is formed by the SD at the moment of the transition of the resonant current through zero (fig. 16).

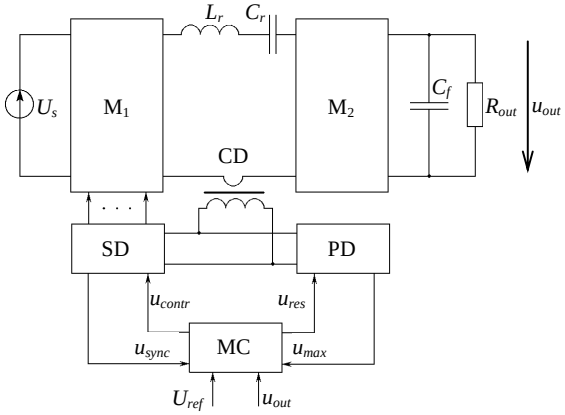

Fig. 15. Functional control circuit of the SRC with pulse-number regulation

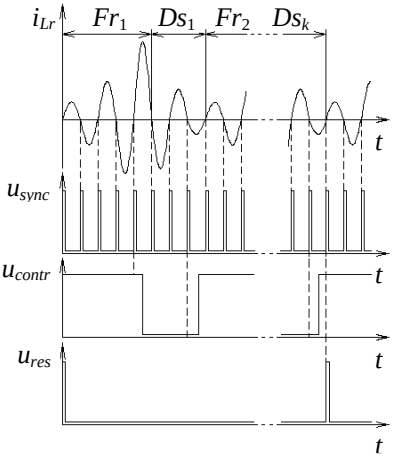

Fig. 16. Time diagrams of the SRC control system with pulse-number regulation

To determine the effectiveness of dividing the main conversion cycle into several small cycles, it is convenient to model the processes in the power part of the power plant using the TCAD application program package. Fig. 17 presents the SRC model with the following parameters: L_r = 128 μH; C_r = 19.8 nF; C_f = 1000 μF; R_{out} = 30 ohms; U_s = 300 V.

Fig. 18 shows the time diagrams of the resonant current (Fig. 18, a) and the resonant capacitor voltage (Fig. 18, b) without dividing the main conversion cycle into small cycles. Current and voltage are given in relative units:

$$u^*_{Cr} = \frac{u_{Cr}}{U_s};\ i^*_{Lr} = \frac{i_{Lr} \cdot \rho}{U_s}.$$

The simulation of the SRC operation was carried out for n_{Fr} = 13 and n = 24. Fig. 18, c shows the time diagram of the resonant current, which is obtained using the state equations of the power circuit of the SRC. Comparison of fig. 18, a and fig. 18, c shows that the presented model of the power section of the SRC corresponds to its mathematical model.

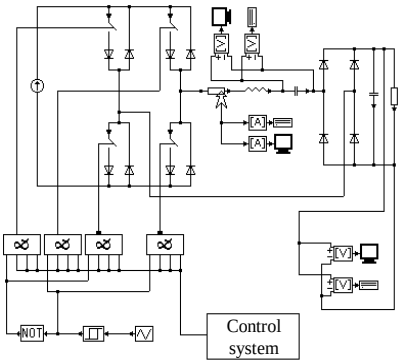

Fig. 17. The model of SRC with pulse-number regulation

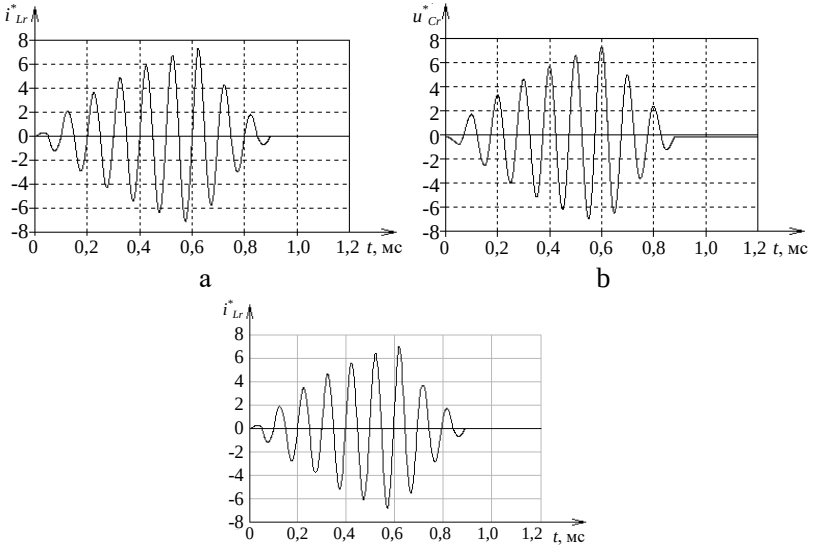

Fig. 6.20. Time diagrams of the resonant current (a) and voltage (b) on the resonant capacitor when using the main conversion cycle and the time diagram of the resonant current obtained using the state equations of the power circuit of the converter (c)

To improve working conditions, the main conversion cycle is divided into 6 small cycles with parameters: $n_{Fri} + n_{Dsi} = 4$, $n_{Fr1} = n_{Fr3} = n_{Fr5} = 3$,

$n_{Fr2} = n_{Fr4} = n_{Fr6} = 2$. Fig. 19 shows the time diagrams of the resonant current (fig. 19, a) and the resonant capacitor voltage (Fig. 19, b) when the main conversion cycle is divided into small cycles.

The time diagrams show that when the main conversion cycle is divided into small cycles, the maximum values of the resonant current and voltage on the resonant capacitor decrease significantly (by a factor of 2). In fig. 18, it is possible to note the time interval during which resonant oscillations stop before the end of the main conversion cycle, which indicates operation in the zone of discontinuous currents. When the main conversion cycle is divided into small cycles, the zone of intermittent currents decreases and, as can be seen from fig. 19, the SRC works in the zone of continuous currents.

The resonance current envelope in fig. 18 contains a harmonic with the frequency of $1/(nT_r)$, and the resonance current envelope in fig. 19 – harmonics with the frequency of $1/((n_{Fri} + n_{Dsi})T_r)$.

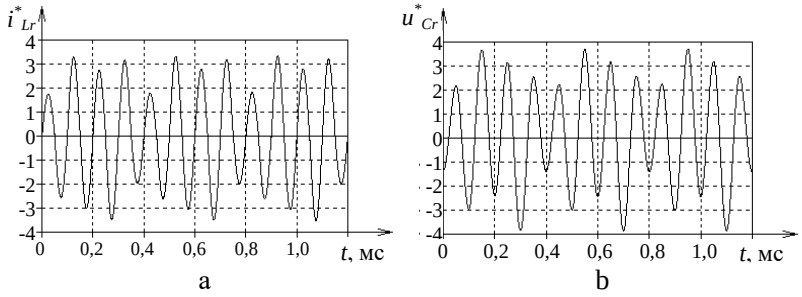

Fig. 19. Time diagrams of resonant current and voltage when the main cycle is broken into small cycles

As $n_{Fri} + n_{Dsi} < n$, then the amplitude of the harmonics of the resonant current envelope when the main conversion cycle is broken down into small cycles is reduced by the output filter more effectively than the harmonics of the resonant current envelope without breaking the main conversion cycle.

The simulation shows the effectiveness of the proposed method of dividing the main conversion cycle into small cycles, which allows to significantly reduce the maximum values of the resonant current and voltage, reduce the pulsations of the current envelope in the resonant circuit and, accordingly, the output voltage.

Fig. 20 shows the load (Fig. 20, a) and control (Fig. 20, b) characteristics of the SRC with pulse-number control. The calculated characteristics are shown by a dashed line.

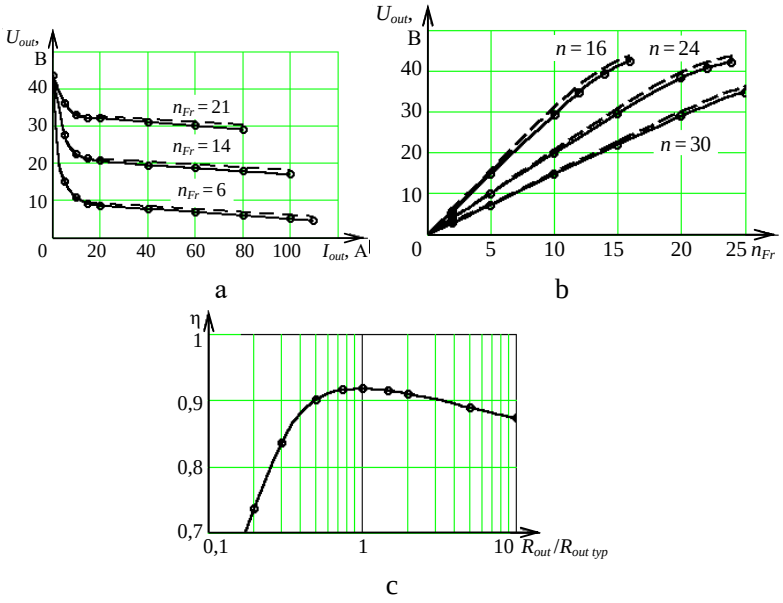

Fig. 20. Load (a) and control (b) characteristics of the PRP with number-pulse control and the dependence of the efficiency coefficient on its relative load (c)

As can be seen from fig. 20, calculated dependences are close to experimental ones. The discrepancy increases in the zone of maximum currents, which is due to the losses of the SRC, which are not taken into account in the calculations.

CONCLUSIONS

Based on the results of own research, the mathematical model of the energy-efficient series-resonant DC/DC converter with pulse-number regulation has been constructed. It allowed to obtain static and dynamic characteristics and study electromagnetic processes in the power section of the SRC for the discontinuous and continuous current modes. The simulation of the SRC operation has shown the effectiveness of the proposed method of dividing the main conversion cycle into small cycles,

which allows to significantly reduce the maximum values of the resonant current and voltage, reduce the pulsations of the current envelope in the resonant circuit and, accordingly, the output voltage. The calculated static characteristics are close to the experimental ones, that confirms the compliance of the developed mathematical model with the real physics of processes in the converter. Thus, the series-resonant converter with pulse-number regulation provides the minimum level of voltage distortions and radio frequency range interference due to the sinusoidal form of currents in the power circuit. The proposed pulse-number method of controlling resonant converters ensures significant reduction of switching losses, energy efficiency increase, and improvement in the conditions of electromagnetic compatibility of converters and power supply.

SUMMARY

In the paper the mathematical model of the energy-efficient series-resonant DC/DC converter with pulse-number regulation has been constructed. The static and dynamic characteristics have been obtained and electromagnetic processes in the power section of the series-resonant converter have been studied. The control system architecture, which implements the pulse-number regulation of the converter's output voltage, has been developed. The simulation of the converter operation has been provided in case of proposed control system use.

BIBLIOGRAPHY

1. Браун М. *Источники питания. Расчет и конструирование*. Киев: «МК-Пресс». 2007. 210 с.

2. Bose B.K. *Modern Power Electronics and AC Drives*. PHI Learning Pvt Lt. 2013. 738 p.

3. Dianbo Fu, Kong P., Wang S., Lee F. C., Ming Xu. Analysis and suppression of conducted EMI emissions for front-end LLC resonant DC/DC converters. *IEEE Power Electronics Specialists Conference.* 2008. Pp. 1144-1150. DOI: 10.1109/PESC.2008.4592084.

4. Pavlov, G., Obrubov, A., Vinnychenko, I. Design procedure of static characteristics of the resonant convertere. *Proc. of IEEE 3rd Ukraine Conference on Electrical and Computer Engineering (UKRCON).* 2021. Pp. 401-406. DOI: 10.1109/UKRCON53503.2021.9575698.

5. Zheng K., Zhang G., Zhou D., Li J., Yin S. Modeling, dynamic analysis and control design of full-bridge LLC resonant converters with sliding-mode and PI control scheme. *Journal of Power Electronics*. 2018.

Vol. 18, no. 3. Pp. 766–777. DOI: https://doi.org/10.6113/JPE.2018.18.3.766.

6. Rubavathy J., Murugesan P. Class D series resonant inverter with PDM scheme for induction heating application. *International Journal of Applied Engineering Research.* 2016. Vol. 11, no. 6. Pp 3819-3827.

7. Павлов Г. В., Обрубов А. В., Нікітіна О. В., Покровський М. В. *Перетворювачі постійної напруги на основі резонансних інверторів: монографія.* Миколаїв: НУК. 2013. 372 с.

8. Pavlov G., Pokrovskiy M., Vinnichenko I. Load characteristics of the serial-to-serial resonant converter with pulse-number regulation for contactless inductive energy transfer. *IEEE 3rd International Conference on Intelligent Energy and Power Systems (IEPS).* 2018. Pp. 133-138. DOI: 10.1109/IEPS.2018.8559590.

Information about the authors:
Pavlov Hennadii Victorovych,
Doctor of Engineering Science, Professor,
Vice-rector for scientific work,
Admiral Makarov National University of Shipbuilding
9, Heroiv Ukrainy ave., Mykolaiv, 54007, Ukraine

Vinnychenko Iryna Leonidivna,
Candidate of Engineering Science, Associate Professor,
Associate Professor
Admiral Makarov National University of Shipbuilding
9, Heroiv Ukrainy ave., Mykolaiv, 54007, Ukraine

Pokrovskii Mykhailo Volodymyrovych,
Candidate of Engineering Science,
Associate Professor
Admiral Makarov National University of Shipbuilding
9, Heroiv Ukrainy ave., Mykolaiv, 54007, Ukraine